RESEARCH ARTICLE | JULY 15 2025

Spatially coherent uniform momentum zones in accelerating turbulent pipe flow

Isuru Gunaratne ; Byron Guerrero ; Martin Lambert ; Rey Chin

Physics of Fluids 37, 075140 (2025)
https://doi.org/10.1063/5.0275275

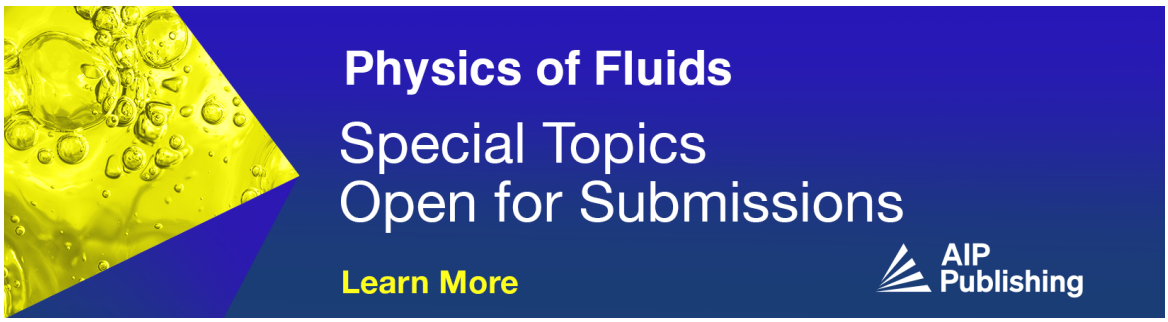

Physics of Fluids ARTICLE pubs.aip.org/aip/pof

Spatially coherent uniform momentum zones in accelerating turbulent pipe flow

Cite as: Phys. Fluids **37**, 075140 (2025); doi: 10.1063/5.0275275
Submitted: 11 April 2025 · Accepted: 23 May 2025 ·
Published Online: 15 July 2025

Isuru Gunaratne,[1,a)] Byron Guerrero,[1,2] Martin Lambert,[3] and Rey Chin[1]

AFFILIATIONS

[1]School of Electrical and Mechanical Engineering, University of Adelaide, Adelaide, South Australia 5005, Australia
[2]Departamento de Ciencias de la Energía y Mecánica, Universidad de las Fuerzas Armadas - ESPE, Sangolquí, Ecuador
[3]School of Civil Engineering and Architecture, University of Adelaide, Adelaide, South Australia 5005, Australia

[a)]Author to whom correspondence should be addressed: isuru.gunaratne@adelaide.edu.au

ABSTRACT

This paper investigates the transient characteristics of spatially coherent uniform momentum zones (UMZs) in an unsteady flow scenario comprising a rapidly accelerating turbulent pipe flow. The current work is based on high-fidelity direct numerical simulation (DNS) data sets starting from an initial friction Reynolds number ($Re_{\tau 0}$) = 500 up to a final friction Reynolds number ($Re_{\tau 1}$) = 670. All instantaneous uniform momentum zones (UMZs) are identified by constructing the probability density functions (PDFs) of the streamwise velocity component of the turbulent flow, as proposed by Adrian *et al.*, "Vortex organization in the outer region of the turbulent boundary layer," J. Fluid Mech. **422**, 1–54 (2000). A rapidly accelerating turbulent pipe flow undergoes four unsteady flow stages: inertial stage, pre-transition stage, transition stage, and finally, core-relaxation stage. The results show that despite the number of flow regions of instantaneous UMZs dropping during the pre-transition stage, more spatially coherent flow regions are seen during the pre-transition stage. Investigation of streamwise length-scales of spatially coherent UMZs reveals that UMZs experience an elongation during the pre-transition stage, followed by a relaxation during the transition and core relaxation stages along the streamwise direction, with UMZs located at different wall-normal locations stretching and relaxing differently. Despite the structural characteristic differences of both instantaneous and spatially coherent UMZs, results indicate that a similar mechanism causes them to either merge or to be annihilated as the flow accelerates, and for them to breakup or reappear as the flow recovers.

I. INTRODUCTION

Uniform momentum zones (UMZs) are large-scale flow structures hierarchically placed within wall-bounded turbulent flows. These structures consist mainly of instantaneous (spatially incoherent) UMZs and spatially coherent UMZs. Spatially incoherent UMZs are short-lived UMZs, while spatially coherent UMZs remain for extended spatial extents of the streamwise flow domain. UMZs have been the center of recent wall-bounded turbulent flow investigations as they allow the investigation of wall-bounded turbulence from a structural perspective, as instantaneous UMZs at different wall-normal locations exhibit drastically different turbulence characteristics.[2] Apart from investigating instantaneous UMZs, researchers have isolated temporally coherent UMZs and conducted studies on these flow structures' temporal evolution for extended time scales.[3] Despite numerous investigations conducted on UMZs, these investigations have been limited to steady turbulent wall-bounded flow conditions, and the need to conduct investigations that focus on UMZs in unsteady flow scenarios is lacking in the currently available research. This work is expected to bridge that gap by isolating and investigating spatially coherent UMZs from instantaneous UMZs in a rapidly accelerating turbulent pipe flow.

A. Accelerating turbulent flow

Deviating from conventional turbulence research characterized by constant bulk flow velocities or, in other words, steady turbulence, researchers have been paying more attention to unsteady turbulence, characterized by time-varying flow rates, as turbulent flows in real-life applications are rarely steady. The center of such unsteady flow research has been turbulent wall-bounded flows containing either a ramp-up increment or a ramp-down decrement in the bulk flow rate of the fluid flow. Numerous experimental and numerical studies have been conducted on this venture to extend the current understanding of

the transient dynamics of accelerating and decelerating turbulent flows. Studies by Maruyama *et al.*,[4] Greenblatt and Moss,[5] He *et al.*,[6] He and Seddighi,[7] He and Seddighi,[8] Mathur,[9] Mathur *et al.*,[10] Guerrero *et al.*,[11] Guerrero *et al.*,[12] and Guerrero *et al.*,[13] are few of such studies to name.

Maruyama *et al.*,[4] were amongst the pioneers to experimentally explore in detail the turbulence response in pipes to sudden changes in the flow rates by imposing step-up increases and step-down decreases in the flow rate. In the step-up scenario of the flow rate, a delayed response in turbulence was seen. They quantified that the "new" turbulence generated by the increase in flow rate is produced at the wall, and it propagates radially to the pipe axis with time. In the step-down scenario of the flow rate, they showed that, similar to the early part of the transient flow, the turbulence intensity decreases monotonically, much like the decay of isotropic turbulence behind a grid. Furthermore, it was mentioned that the linear decay law applies to the decay in the transient pipe flow, and the radial dependence of the decay rate is proportional to its initial steady value.

The experimental work by Greenblatt and Moss[5] of rapidly accelerating turbulent pipe flows utilizing single-component laser-Doppler velocimeter (LDV) techniques revealed that a rapidly accelerating turbulent pipe flow exhibits three unsteady phases: initial, final, and relaxation. Furthermore, coherence was displayed by the resultant flow displacement and momentum thickness as they developed over time. Numerical investigations conducted by He and Seddighi[7] on a transient channel flow following a rapid increase in the flow rate showed that the flow development undergoes three phases: pre-transition, transition, and fully turbulent. Extending on the findings of this study and overcoming the limitation of relatively low friction Reynolds numbers ($Re_\tau = 180 - 418$), Guerrero *et al.*[11] and Guerrero *et al.*[13] investigated rapidly accelerating and rapidly decelerating turbulent pipe flows between two steady Reynolds numbers. They identified four transient flow stages in accelerating and decelerating cases, but with distinctly different flow characteristics. For the accelerating flow, the four stages identified by the authors were the inertial, a stage displaying frozen turbulence and a rapid increase in viscous forces; pre-transition, a rapid reduction of viscous forces with a weak response to turbulence in the near wall region; transition, a steady increment of turbulent inertia and viscous forces in the inner region; core relaxation, reconstitution of the wake region due to turbulence transport by diffusion and advection.

For the decelerating flow, the four stages identified by the authors were the inertial, a stage displaying contrasting behavior of turbulent inertial and viscous forces with a mild decay of turbulent inertia and rapid response of viscous forces (viscous forces change its sign from negative to positive) within the viscous sub-layer region; friction recovery, a stage where viscous forces seem to gain substantial recovery and overshoot their final steady state while turbulent inertia seems to undergo a progressive decay close to the wall (near wall region) and eventually overshoot its final steady value at the buffer region; turbulence decay, a stage of balanced decay of both turbulence inertia and viscous forces; core relaxation, a stage of attending a quasi-steady state and this stage similar to the acceleration case, extends to an extensive period with the wake region slowly recovering.

B. Flow structures in wall-bounded turbulence

With the growing advancements in fluid mechanics, significant efforts have been made to investigate the structural organization of wall-bounded turbulence. The pioneering investigations by Theodorsen[14] were one of the first studies to identify horseshoe vortex structures in wall-bounded turbulent flows. They detected that these vortical structures originate at the wall, with an inclination of approximately 45° with the wall. Kline *et al.*[15] focused on the near wall low-speed streak formation, and they were amongst the first to link the interactions between these low-speed streaks to the transport of turbulent kinetic energy of the bulk flow. Following work by Theodorsen[14] and Head and Bandyopadhyay[16] were able to provide impeccable evidence into the occurrences of vortical structures (horseshoe and hairpin vortices) in turbulent boundary layers and were able further to show the Reynolds number dependence of these structures. They were able to show that at low Reynolds numbers ($Re_\theta < 800$), where Re_θ is the Reynolds number based on the momentum thickness θ, the separation of scales is slight, and the shapes of these structures are not distinct. Furthermore, once investigated at higher Reynolds numbers ($Re_\theta > 2000$), they observed that these structures had undergone an elongation, providing conclusive evidence of a possible Reynolds number effect on vortical structures in wall-bounded turbulence.

Following the pioneering work by Brown and Thomas,[17] the focus of analyzing the structural organization of wall-bounded turbulence shifted from single structures (such as horseshoe and hairpin vortices) to large-scale structures that formed bulges reaching up to 2–3 δ, where δ is the boundary layer thickness. These coherent structures were widespread within the logarithmic region up to the wake region of the flow. Following this study, Christensen and Adrian,[18] Ganapathisubramani *et al.*,[19] and Adrian[20] conducted in-depth investigations to study the characteristics of large-scale motions (LSMs) of a similar order of streamwise extent and Kim and Adrian[21] investigated very large-scale motions (VLSMs) in wake regions of pipes of streamwise extent reaching up to 12–14 R, where R is the radius of the pipe.

C. Uniform momentum zones

As researchers were pursuing investigations with regard to LSMs and VLSMs in wall-bounded turbulence, Meinhart and Adrian[22] were amongst the first to observe a zone-like structural organization of a boundary layer flow, and the unique characteristic seen of these zones was that these were regions with similar streamwise momentum and these regions were bound by regions of intensified shear and vortical activity. They would proceed to name these flow regions as uniform momentum zones (UMZs) and the boundaries of UMZs as internal shear layers (ISLs). Adrian *et al.*,[1] proposed characterizing UMZs based on the peaks of the probability density functions (PDFs) constructed based on the streamwise velocity of the turbulent flow.

Apart from the PDF approach proposed by Adrian *et al.*,[1] UMZs have been identified by isolating local regions of high shear (internal shear layers) within the flow. These internal shear layers (ISL) correspond to the boundaries of UMZs, and the ISL method has overcome significant limitations of the PDF method since it does not rely on user-defined parameters and the streamwise domain length in identifying regions of similar streamwise momentum.[23] To demonstrate its advantages, Chen *et al.*,[23] followed an ISL approach in identifying UMZ based on the peaks of the instantaneous streamwise velocity profile and the corresponding velocity gradient profiles. Gul *et al.*,[24] investigated UMZs based on a three-dimensional ISL detection criteria defined around vortex sheets, using the A_+ criterion proposed by Horiuti and Takagi.[25] These internal shear layers or vortex sheets are

flow regions with high vorticity and strain rate correlations. Apart from the PDF and ISL-based methods, a kernel density estimation (KDE) method consisting of a single KDE bandwidth was proposed by Fan *et al.*,[26] and this method eliminates the need for multiple user-defined thresholds, which are needed for the PDF-based method.

Although UMZs were initially characterized to be primarily seen in turbulent boundary layer flows, Kwon *et al.*[27] were able to investigate UMZs in a turbulent channel flow by focusing on the quiescent core of the flow. A distinct jump in turbulence statistics was seen in their results as the core boundary is crossed from flow regions inside the quiescent core to flow regions outside the quiescent core, which led them to compare the quiescent core boundary to the turbulent/non-turbulent interface of boundary layer flows.[27] In turbulent boundary layer flows, De Silva *et al.*,[28] were able to show that a log-linear relationship exists between the average number of UMZs (N_{UMZ}) and the Reynolds number of the bulk flow. Furthermore, they showed that UMZs seen away from the wall are thicker than UMZs seen near the wall. More recently, Chen *et al.*,[2] and Chen *et al.*,[23] investigated UMZs in turbulent pipe flows. Apart from these investigations, UMZs have been investigated extensively, experimentally, and numerically, in wall-bounded steady turbulent flow research. In a rapidly accelerating turbulent pipe flow, Guerrero *et al.*,[11] investigated the quiescent core of the pipe and showed that it displayed a delayed turbulence response to the flow excursion. Furthermore, the quiescent core propagated alongside the flow, maintaining its geometry. This behavior is similar to an independent plug flow.

Laskari *et al.*[3] were amongst the pioneers in tracking UMZs in time by investigating the temporal behavior of UMZs seen within a turbulent boundary layer flow. They tracked UMZs within a fixed field of view (FOV) in consecutive snapshots in time and isolated temporally coherent UMZs based on the zone modal velocity (u_m) of each UMZ. They were able to show that flow regions consisting of a higher than average number of zones are a result of a large-scale $Q2$ event in the log region, and flow regions consisting of a lower than average number of UMZs are a result of a large-scale $Q4$ event in the log region. Furthermore, they showed that flow regions with a lower-than-average number of zones remain temporally coherent longer within the FOV than those with higher-than-average zones.

The motivation of the current study is to isolate spatially coherent UMZs from all detected instantaneous UMZs and to investigate the behavior of these long-lived, large-scale flow structures in a rapidly accelerating turbulent pipe flow from a structural point of view. The structure of the current work is as follows. Proceeding with the introduction in Sec. I, the accelerating flow parameters, the detection scheme for instantaneous UMZs, and the isolation scheme of spatially coherent UMZs are summarized in the methodology section in Sec. II. The results are presented and discussed in Sec. III, and finally, the conclusions of the current work are provided in Sec. IV.

II. METHODOLOGY

Based on high-fidelity volumetric data sets obtained from Guerrero *et al.*,[11] the current authors investigate spatially coherent UMZs filtered from instantaneous UMZs for each temporal instance of the flow. The reason for isolating spatially coherent UMZs from instantaneous UMZs is that these large-scale flow structures remain seen for extended flow regions and represent prominent UMZs. Instantaneous UMZs are identified based on the PDF method proposed by Adrian *et al.*[1] Spatially coherent UMZs are filtered from instantaneous UMZs based on the isolation scheme followed by Laskari *et al.*[3] in isolating temporally coherent UMZs. The high fidelity datasets were generated using the spectral element solver Nek5000,[29] run on a periodic spectral mesh of seventh-order Gauss–Labatto–Legendre (GLL) quadrature points. The $P_N P_N$ solver algorithm of Nek5000[29] was utilized to resolve the incompressible Navier–Stokes equations. A third-order backward difference scheme (BDF3) was implemented for temporal integration of the momentum and continuity equations. For further information regarding the numerical schemes followed while acquiring the turbulent transient data, readers are referred to Guerrero *et al.*,[30] and Guerrero *et al.*,[11] The rapidly accelerating pipe flow parameters are summarized in Table I.

The friction Reynolds number, i.e., Re_τ is defined as $Re_\tau = u_\tau R/\nu$, where R is the pipe radius and ν is the kinematic viscosity of the fluid. The friction velocity $u_\tau = \sqrt{\tau_w/\rho}$, where τ_w is the mean wall shear stress of the fluid. The "+" superscript corresponds to normalization in viscous units with indices "0" and "1" denoting normalization in viscous units concerning the initial and the final states of steadiness attained by the transient flow after undergoing acceleration. The "ramp," "samp," and "sim" subscripts correspond to the ramp-up (acceleration) time, the sampling time interval of data stored, and the DNS simulation duration, respectively. γ is a non-dimensional ramp rate parameter that incorporates the bulk velocity U_b of the flow, where $\gamma = [dU_b/dt)(1/U_{b0})(D/u_{\tau 0})]$ as introduced by He and Jackson.[31] A γ value of $\gamma \gg 1$ ensures that the flow deviates from any pseudo-steady behavior as the flow is accelerated.[31] This confirms that the skin friction coefficient C_f peaks and plateaus during the flow excursion as shown in Fig. 1. The variables z, θ, and r denote streamwise, azimuthal, and radial directions, respectively, and $y = -r$ is the wall-normal direction. L_z corresponds to the streamwise flow domain extent. Finally, Δz^+, $\Delta R\theta^+$, and Δy^+ are the grid resolution of the spectral mesh implemented by Guerrero *et al.*,[11] respectively.

The timescales for each transitional flow stage identified by He and Seddighi[7] and Guerrero *et al.*[11] of the unsteady flow were identified from the temporal evolution of the skin friction coefficient C_f as in Fig. 1. The inertial stage starts when the flow is accelerated at $t^{+0} = 0$ and finishes at the peak attained by C_f. During the pre-transition stage, C_f decays, and according to He and Seddighi,[7] it finishes when C_f has attained a minimum. The transition stage is defined from its minimum to when C_f overshoots the final steady state. Finally, the core relaxation stage is defined for the timescales where C_f

TABLE I. Computational parameters from Guerrero *et al.*[11]

$Re_{\tau,0}$	$Re_{\tau,1}$	Δt^{+0}_{ramp}	Δt^{+0}_{samp}	Δt^{+0}_{sim}	γ	Δz^{+1}	$\Delta R\theta^{+1}$	Δy^{+1}_{wall}	Δy^{+1}_{core}	*Grid points*	L_z/R
500	670	11.8	0.6	894.64	34.36	7.4	6.3	0.05	7.5	328×10^6	8π

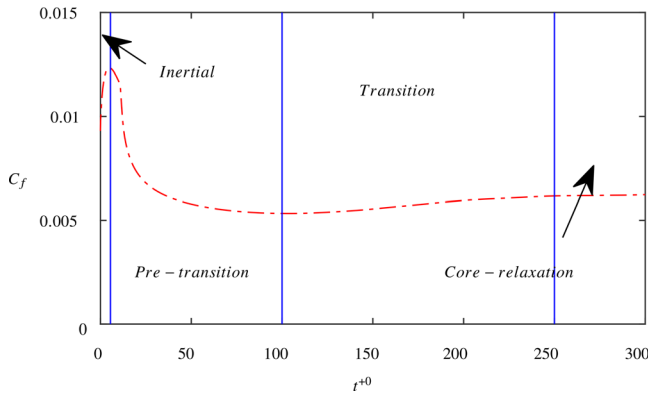

FIG. 1. Temporal evaluation of the skin friction coefficient C_f. Dashed-dotted line (— · —) depicts data from the current study. Timescales of unsteady flow stages from Table II are depicted by (———) for the reader.

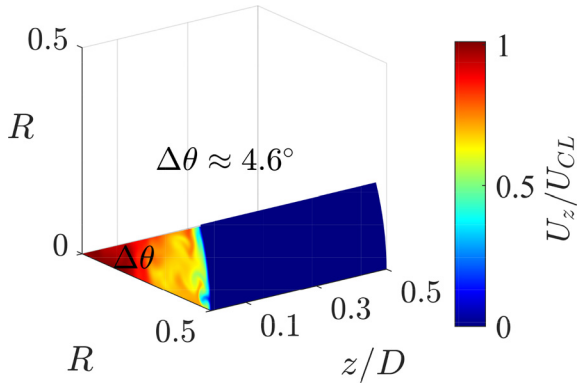

FIG. 2. 3D volumetric flow data slice.

remains quasi-steady while the wake evolves toward its final steady state. The results of the time scales identified for the current flow in Fig. 1, based on the flow parameters set in Table I, are summarized in Table II.

A. Detection of instantaneous UMZs and isolation of spatially coherent UMZs

1. Instantaneous UMZs

Following the methodology proposed by Adrian *et al.*,[1] a PDF-based approach was implemented for the current work, similar to De Silva *et al.*[28] and Chen *et al.*[2] Instantaneous UMZs were identified by constructing the PDF for the instantaneous streamwise velocity U_z from rapidly accelerating turbulent pipe flow fields. Similar to De Silva *et al.*[28] and Chen *et al.*,[2] the peaks of the PDFs are characterized as the zone modal velocities (u_m) of the UMZs and as defined by Chen *et al.*,[2] the minimum PDF values between two consecutive peaks are characterized as the boundaries of UMZs (u_k). Volumetric wedges of U_z with an azimuthal extent of $\Delta\theta \approx 4.6^{\circ}$ and a streamwise extent (streamwise window size) of $0.5R$ were investigated along the flow domain (refer to Appendix in Sec. IV for the rationale behind the current author's wedge dimension selection and the detailed sensitivity test conducted in selecting the appropriate azimuthal extent of the wedge). A three-dimensional (3D) streamwise flow data utilization along the flow domain of $0.5R$ windows for a given snapshot is indicated in the example flow visualization in Fig. 2. Here, the azimuthal extent of Fig. 2 is up scaled by five times to provide a better visualization and added clarity to the reader.

At each streamwise window of size $0.5R$, independent wedges are placed along the azimuthal direction, with each wedge covering approximately 4.6° of azimuthal space (10 grid points). Once a $0.5R$ streamwise window of interrogation is completed at a L_z/R location, the identification process is repeated by moving the interrogation window a single grid point along the streamwise direction, corresponding to $L_z/R + \Delta z/D$, where $\Delta z/D$ is the distance between two streamwise grid points. In total, 8470 wedges were utilized.

A uniform bin size for the PDFs was defined, with each bin representing 1% U_z/U_{CL}, where U_{CL} is the local mean centerline velocity for each instantaneous flow field, and it was used to normalize all U_z values so that $U_z/U_{CL} \in (0,1.1)$.

A peak isolation scheme was then defined similarly to Chen *et al.*,[2] with three distinct constraints, F_d, F_h, and F_p. F_d is the minimum gap between adjacent local PDF peaks in scales of bins, F_h is the minimum PDF value of local PDF peaks to be considered a UMZ, and F_p is the minimum percentage of prominence compared to the average of 10% neighboring PDF values of five bins on each side of the local peak. The threshold values set for the current analysis are provided in Table III.

An example depiction of instantaneous UMZs identified based on the PDF of U_z is provided in Fig. 3(a), and the corresponding $R-\theta$ contour of the identified UMZs is provided in Fig. 3(b).

2. Spatially coherent UMZs

Once all instantaneous UMZs were extracted, the characterization of spatially coherent UMZs from all instantaneous occurrences of UMZs was conducted. Similar to the definition of time-coherent zones by Laskari *et al.*,[3] instantaneous UMZs whose zone modal velocities u_m values remain within a buffer range of $\pm 1\%\ U_z/U_{CL}$ in consecutive investigation windows along the flow domain of a given time instance are defined as spatially coherent UMZs.

Here, a change in $\pm 1\%\ U_z/U_{CL}$ corresponds to a shift in the PDF peak by a single bin due to the uniform bin size used in constructing the PDFs. Figure 4(a) provides the filtered PDF of spatially coherent UMZs, while Fig. 4(b) highlights spatially coherent and incoherent UMZs identified from Fig. 4(a). Regions contoured with solid colors

TABLE II. Timescales for each transitional stage in the current study.

Stage	Inertial	Pre-transition	Transition	Core-relaxation
Timescale	$0 < t^{+0} \lesssim 10$	$10 < t^{+0} \lesssim 100$	$100 < t^{+0} \lesssim 250$	$t^{+0} \gtrsim 250$

TABLE III. The threshold values set for instantaneous UMZ identification.

Symbols	Values
F_d	3% U_z/U_{CL}
F_h	0.5
F_p	25%

red, yellow, and magenta represent flow regions filtered as spatially coherent UMZs. In contrast, the flow region contoured with gray represents the flow region filtered as a spatially incoherent UMZ.

Expanding the filtration of spatially coherent and incoherent UMZs from Fig. 4(b) along the streamwise flow domain, Fig. 5 provides an overview of the flow domain filtered results obtained of spatially coherent and incoherent UMZs identified. Here, the initially steady turbulent flow field at $t^{+0} = -2.8138$ is considered. Similar to Laskari *et al.*,[3] gray squares represent short-lived, spatially incoherent UMZs, while the colored squares represent long-lived, spatially coherent UMZs. Taking a step further, UMZs are colored based on the rank of UMZs based on their zone modal velocities (u_m) due to the hierarchical arrangement of these flow regions.[2] UMZ ranks only up to six zones are considered, with red squares representing the fastest UMZs located furthest from the wall (UMZ 1), yellow squares representing the second fastest UMZs (UMZ 2), green squares representing the third fastest UMZs (UMZ 3), magenta squares representing the fourth fastest (UMZ 4), cyan squares representing the fifth fastest (UMZ 5), and blue squares representing the sixth fastest, most near-wall UMZs (UMZ 6). From the filtered results, it is evident that UMZ 1, UMZ 2, and UMZ 3, depicted by red, yellow, and green squares, tend to be mostly spatially coherent (UMZ 1 being the most spatially coherent), while UMZ 4, UMZ 5, and UMZ 6, depicted by magenta, cyan, and blue squares, respectively, tend to be mostly spatially incoherent. Kwon *et al.*[27] were able to show that the quiescent core of a turbulent channel flow extends up to half of the domain length, and since UMZ 1 primarily resembles the quiescent core of a pipe,[11] this result is in agreement with the findings by Kwon *et al.*[27] Satisfied by the spatially coherent and incoherent UMZ results obtained at the initially steady flow field based on the proposed filtration methodology, we then proceed to investigate the statistics of spatially coherent UMZs as the flow is rapidly accelerated.

Figure 6 provides the PDF distribution of the spatially coherent number of UMZs ($N_{\widetilde{UMZ}}$) extracted from all instantaneous UMZs and the PDF distribution of the number of instantaneous UMZs. The peak was found for all instantaneous UMZs (N_{UMZ}) at $N_{UMZ} = 5$, and the peak for the filtered spatially coherent UMZs was found at $N_{\widetilde{UMZ}} = 3$ from the initial steady base flow (Fig. 6). The distribution for all instantaneous UMZs agrees with the distribution reported by Chen *et al.*,[2] where the turbulent flow characteristics from their study are similar to the initial base flow characteristics of the current work. Furthermore, it is crucial to pay attention to periodicity errors when investigating turbulence statistics extracted from numerical studies containing periodic boundary conditions at either end of the simulation domain.[32] Hence, when investigating UMZs (and spatially coherent UMZs), to avoid any periodicity errors in measurements such as the length scale measurements, only the streamwise extent L_z of $\pi R \leq L_z \leq 7\pi R$ was used instead of the entire flow domain available ($0 \leq L_z \leq 8\pi R$).

Throughout the preceding sections of the current study, we compare the PDFs of spatially coherent and incoherent UMZ

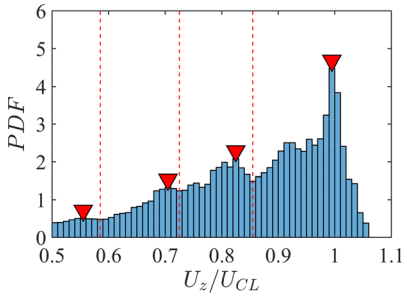

(a) Instantaneous UMZs detected.

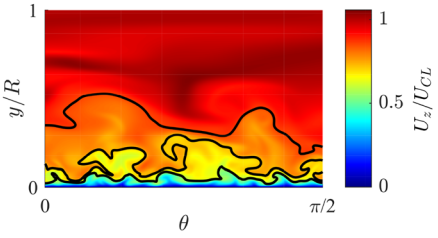

(b) The unwrapped $R-\theta$ contour of the detected instantaneous UMZs.

FIG. 3. (a) An example PDF of U_z for a window size of 0.5R. The red dashed lines (— —) depict the boundaries with ▼, depicting the zone modal velocities of UMZs. The solid black lines (—) depict all boundary contours of UMZs. (b) The corresponding unwrapped $R-\theta$ contour of the detected instantaneous UMZs from 3(a).

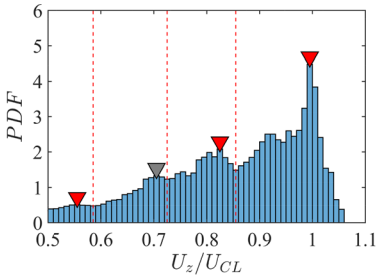

(a) Filtered PDF of spatially coherent UMZs.

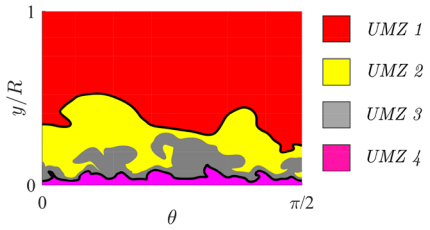

(b) The corresponding unwrapped $R-\theta$ contour of spatially coherent UMZs from 4(a).

FIG. 4. (a) An example PDF of U_z for a window size of 0.5R. The red dashed lines (— · —) depict the boundaries with ▽, representing spatially incoherent zone modal velocities of UMZs. (b) The $R-\theta$ contour of spatially coherent UMZs with spatially incoherent flow region highlighted in solid gray (UMZ 3).

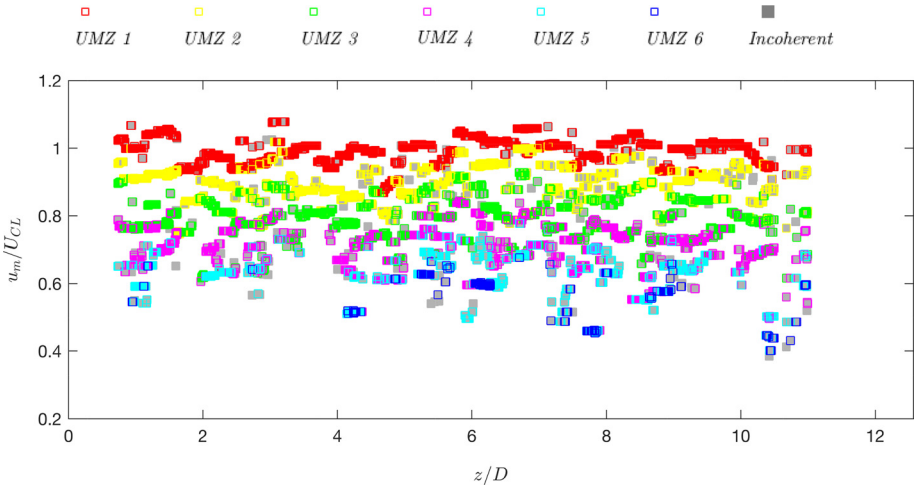

FIG. 5. Filtered spatially coherent UMZs along the entire flow domain. Gray squares ■ depict spatially incoherent UMZs while colored squares represent spatially coherent UMZs.

characteristics extracted, and a suitable test to verify that the distributions are distinct was necessary. The well-known Kolmogorov–Smirnov (KS) test was conducted between all PDF distributions of length-scales of spatially coherent UMZ 1–6 and the N_{UMZ} of instantaneous and spatially coherent UMZs $N_{\widetilde{UMZ}}$, and based on the test results, they were confirmed to be distinct with p values < 0.005 and KS values > 0.1, hence rejecting the null hypothesis, confirming that indeed the distributions are significantly different.

III. RESULTS AND DISCUSSION

A. The transient nature of the probability density function of N_{UMZ}

The behavior of the PDFs of N_{UMZ} captured during the four transitional stages of the accelerating flow are investigated in this section. Figures 7 and 8 provide the results obtained alongside the timescales the data were computed at for both instantaneous UMZs and spatial UMZs. For both the figures, arrows indicate the significant trends seen with progressing time. First, we investigate the instantaneous N_{UMZ} trends. As seen in Fig. 7(a), during the inertial stage, a sudden drop occurs in flow regions where $N_{UMZ} \geq 5$, while more flow regions with $N_{UMZ} \leq 5$ are seen. Toward the end of the inertial stage, the peak shifts from 5 to 4. Based on these results, it is evident that complex flow structures containing higher N_{UMZ} are being annihilated, while regions with lower N_{UMZ} become more common toward the end of the inertial stage. This result agrees with the laminarescent trend seen in accelerating flows as shown by Narasimha and Sreenivasan[33] and He and Seddighi.[7] As the flow transitions to the next stage in Fig. 7(b), i.e., the pre-transition stage, the peak of the distribution continues to increase at 4, indicating flow regions with $N_{UMZ} \geq 4$ are becoming less. Flow regions with $N_{UMZ} \geq 6$ become rare. It is reasoned by He and Seddighi[7] and He and Seddighi[8] that there is a decrease in turbulence near the wall as the turbulent transient flow tends to relaminarize itself during the pre-transition stage, which causes flow regions with high N_{UMZ} to dynamically reallocate themselves to flow regions of lower N_{UMZ} away from the wall. As seen in Fig. 7(c), although the peak remains at 4 during the transition stage, more flow regions with $N_{UMZ} \geq 5$ become abundant, while flow regions with $N_{UMZ} \leq 5$ become less seen. This is caused by the additional complex flow patterns created due to the propagation of the newly generated turbulence from the near-wall region, which enhances the turbulence levels in the flow. As in Fig. 7(d), toward the end of the reported time instances of the core-relaxation stage, the flow recovers with the peak returning to 5, similar to the distribution prior to the flow acceleration.

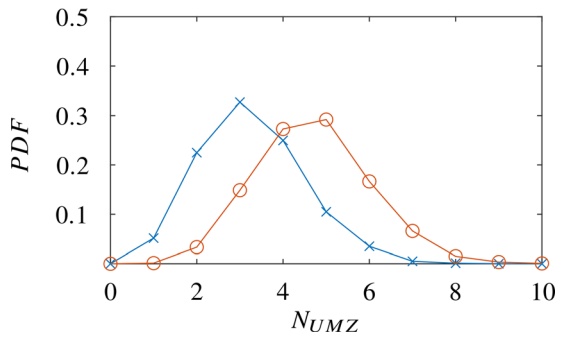

FIG. 6. Probability density function of the number of instantaneous N_{UMZ} and spatially coherent $N_{\widetilde{UMZ}}$ UMZs detected. Solid line (———) with circular markers (○) depicts all detected instantaneous UMZs, while the solid line (———) with cross markers (×) depicts spatially coherent UMZs at $t^{+0} = -2.8138$ (negative sign for initial steady state).

Next, we investigate the trends seen in spatially coherent $N_{\widetilde{UMZ}}$ as shown in Fig. 8. In Fig. 8(a), a frozen behavior is seen with $N_{\widetilde{UMZ}}$ during the inertial stage, indicating that flow regions with spatially coherent flow structures tend not to change. Based on the findings by Kwon *et al.*[27] and Chen *et al.*,[2] the fastest UMZs are located furthest from the wall of the channel/pipe flow, and they predominately are the spatially coherent flow structures within the flow domain, often stretching up to half the flow domain length.[27] As spatially coherent flow structures are seen untethered during the inertial stage, this result agrees with the findings by He and Seddighi[7] and He and Seddighi,[8] where they showed that the laminarescent behavior is predominant in the near-wall region and tends to annihilate near-wall flow structures. Based on this result, it can be concluded that the laminarescent trend seen in accelerating flows, as shown by Narasimha and Sreenivasan[33] and He and Seddighi,[7] does not seem to affect spatially coherent UMZs.

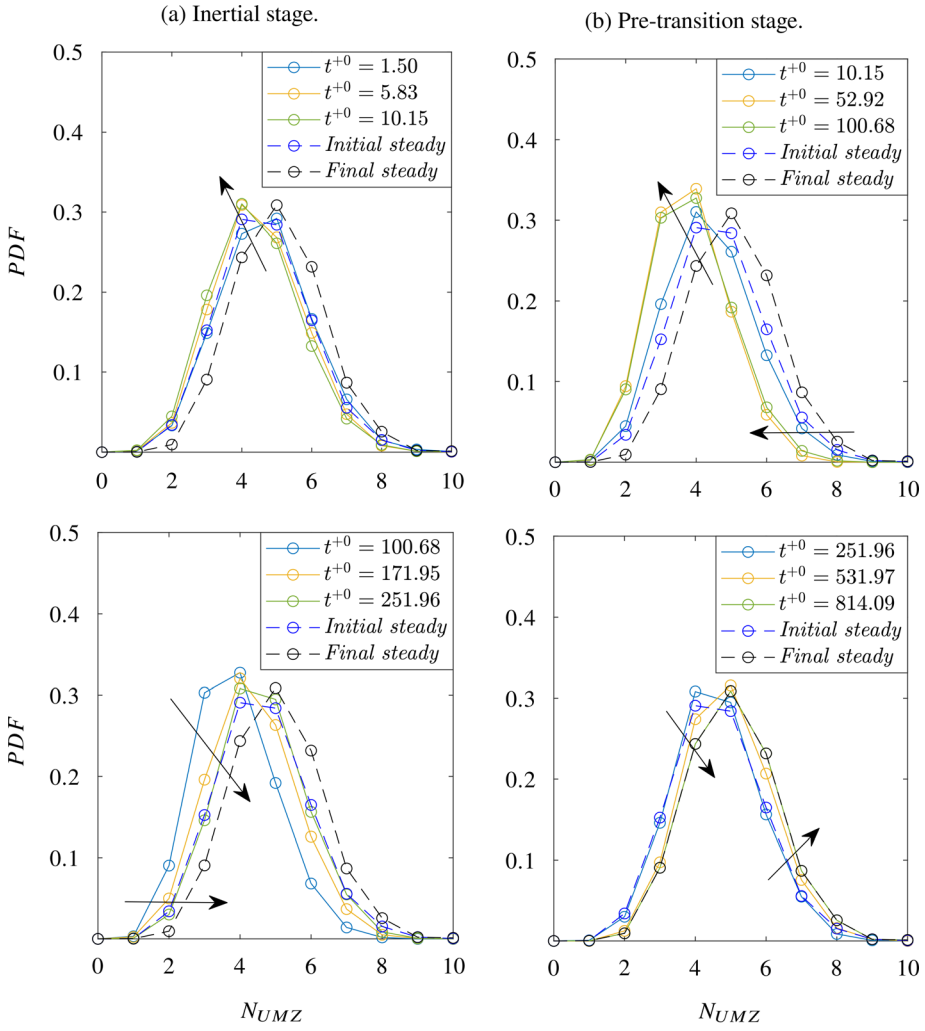

FIG. 7. PDF of N_{UMZ} for all instantaneous UMZs detected during the (a) inertial, (b) pre-transition, (c) transition, and (d) core-relaxation stages of the transient turbulent flow. Arrows point toward trends observed with progressing time.

However, the laminarescence observed during the pre-transition seems to annihilate some of the instantaneous UMZs during the inertial stage.

As the flow transitions to the pre-transition stage in Fig. 8(b), an increase in the peak is seen, while the peak $N_{\widetilde{UMZ}}$ remains at 3. As the peak increases in value, a rapid drop in flow regions representing spatially coherent UMZs with $N_{\widetilde{UMZ}} \geq 3$ is seen, while an increase in spatially coherent flow regions is seen with $N_{\widetilde{UMZ}} \leq 3$. This behavior is similar to instantaneous UMZs and the drop in turbulence levels near the wall as the flow tends to relaminarize effects of the spatially coherent UMZs located nearest to the wall, causing them to reallocate themselves into flow regions with lower $N_{\widetilde{UMZ}}$. As shown in Fig. 8(c), during the transition stage, the peak value of $N_{\widetilde{UMZ}}$ drops at 3, flow regions with $N_{\widetilde{UMZ}} \geq 3$ experience an increase, and flow regions with $N_{\widetilde{UMZ}} \leq 3$ become less abundant. Finally, as shown in Fig. 8(d), toward the end of the core-relaxation stage, spatially coherent UMZs settle toward their initial steady flow distribution, with peak $N_{\widetilde{UMZ}} = 3$. Based on this result and the results from the two previous stages, i.e., pre-transition and transition stages, it can be stated that spatially coherent and incoherent UMZs behave similarly during the pre-transition, transition, and core-relaxation stages, with the turbulence propagation from the wall affecting $N_{\widetilde{UMZ}}$ and N_{UMZ} in a similar manner. In other words, this result indicates that a similar underlying mechanism affects spatially coherent UMZs and incoherent UMZs to reallocate into less densely packed flow regions and vice versa during the unsteady flow stages.

In order to further investigate this underlying mechanism, we then investigate the total number of N_{UMZ} and $N_{\widetilde{UMZ}}$, instead of the normalized PDF distribution to get a better understanding of whether there is indeed a drop in these flow regions. Figure 9 provides the total number of flow regions recorded as the flow transitions through the four unsteady flow stages. It is seen that there is indeed a drop of the total number of flow regions seen for both spatially coherent $N_{\widetilde{UMZ}}$ and instantaneous N_{UMZ}, indicating a possible merging or an annihilating mechanism of UMZs. This drop is seen during the inertial and pre-transition stages and as explained by He and Seddighi,[7] Guerrero

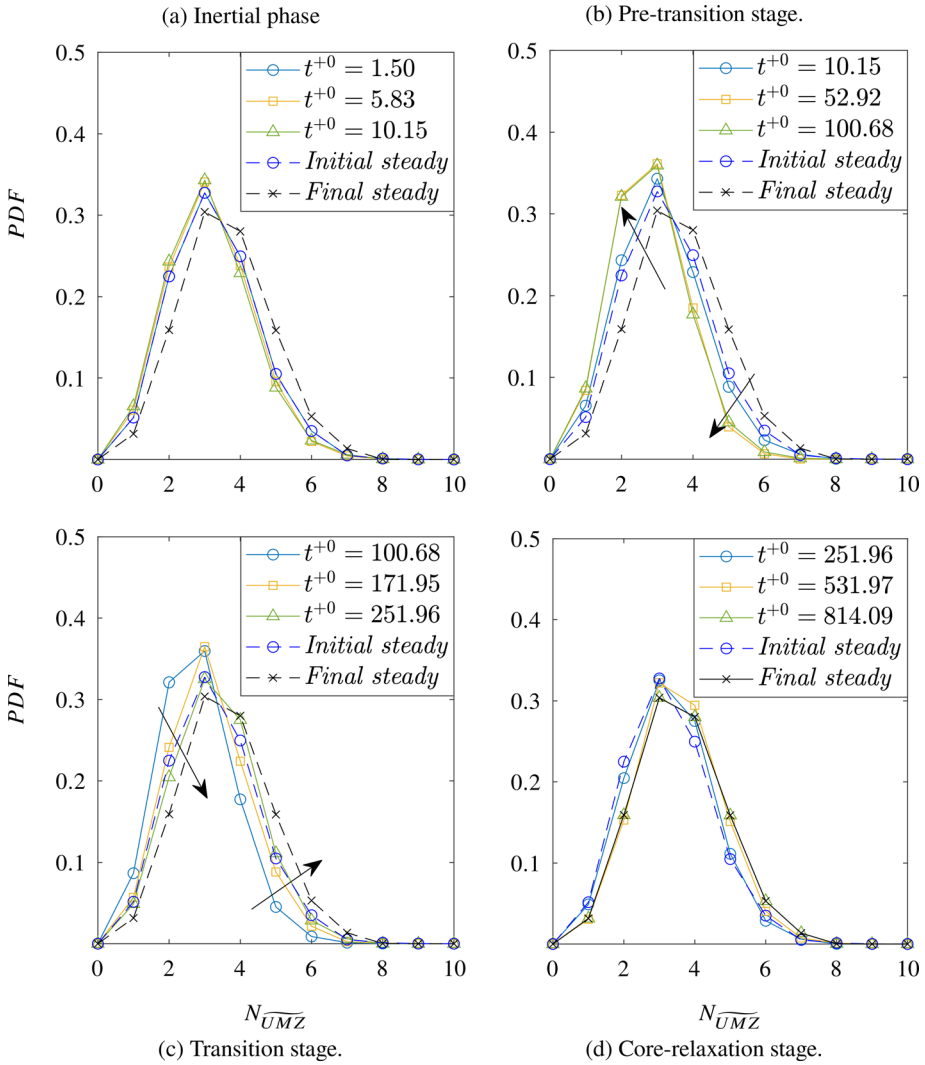

FIG. 8. PDF of $N_{\widetilde{UMZ}}$ detected during the (a) inertial, (b) pre-transition, (c) transition, and (d) core-relaxation stages of the transient turbulent flow. Arrows point toward trends observed with progressing time.

et al.,[11] and Guerrero *et al.*,[12] a laminarescent trend was observed during the inertial and pre-transition stages. Therefore, it is likely to observe a drop, signifying less unstable and more stable UMZs during these stages. For clarity, only timescales up to $t^{+0} = 300$ are shown in Fig. 9. Toward the end of the recorded timescales, i.e., $t^{+0} = 840$, the total number of zones reach values similar to their initial values prior to the flow excursion (not shown in Fig. 9).

B. Length-scales on UMZs

In the literature on flow structures, it is well documented that flow structures elongate and shorten as a response to changes in the bulk Reynolds number of the flow.[7,8,11] Guerrero *et al.*,[11] and He and Seddighi[7] were able to show that flow structures elongate toward the end of the pre-transition stage and tend to relax toward the end of the transition stage by conducting two-point correlations along the streamwise direction of the flow. To further investigate how individual UMZs behave, we investigate the temporal evolution of length-scales of the six fastest spatially coherent UMZs. It is emphasized that to avoid any periodicity errors in the analysis, length-scales are extracted only within $\pi R \leq L_z \leq 7\pi R$, instead of the entire flow domain available ($0 \leq L_z \leq 8\pi R$). The spatially coherent UMZ length-scales are extracted using a moving interrogation window of $0.5R$ slice by slice within the streamwise length $\pi R \leq L_z \leq 7\pi R$ as shown in Fig. 2.

Figure 10(a) represents the PDF of length-scales distribution of the fastest UMZs, i.e., UMZ 1, during the inertial stage of the flow. Before the flow acceleration, the average spatial extent along the pipe axis of these spatially coherent structures is $z/D \approx 3.2$, with considerable length-scales extending beyond the effective half domain length ($7\pi/2$). The overall length-scales range within the range of $0.9 \geq z/D \geq 9.3 (\approx 7\pi/2)$. This result is similar to the findings by Kwon *et al.*,[27] where the quiescent core of a channel flow extends to half the domain length. Since UMZ 1 mostly resembles the quiescent core, the length-scales extracted from the current work do show agreement with this result. As shown in Fig. 10(a), the length scale distribution was found not to fluctuate much until toward the end of the

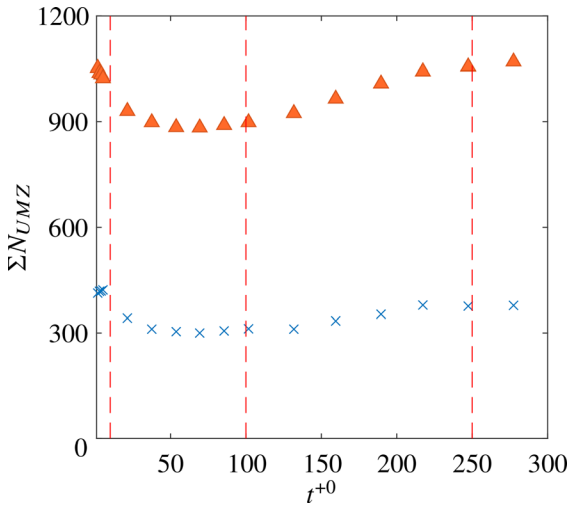

FIG. 9. A comparison of the total number of instantaneous N_{UMZ} (▲) and spatially coherent $N_{\widetilde{UMZ}}$ (×) UMZs detected at each temporal instance.

inertial stage ($t^{+0} \approx 5.83$). Toward the end of the inertial stage, it is seen that the spatially coherent UMZs are starting to stretch as the peak of the distribution shifts to $z/D \approx 3.4$. Figure 10(b) represents the PDF of the length-scales distribution of UMZ 1 during the pre-transition stage of the flow. Following the trend toward the end of the inertial stage, spatially coherent UMZ 1 extends its streamwise spatial length-scales. The peak of the distribution drops and shifts to $z/D \approx 3.9$ from $z/D \approx 3.4$ while broadening itself, indicating that more coherent structures are experiencing elongation. Figure 10(c) represents the PDF of the length-scales distribution of UMZ 1 during the transition stage of the flow. During this stage, the opposite trends are seen from the pre-transition stage, where the spatially coherent UMZ 1 is seen to elongate. During the transition stage, UMZ 1 is seen settling at an average streamwise extent of $z/D \approx 3.9$.

As the flow transitions to the final stage depicted by Fig. 10(d), i.e., the core-relaxation stage, the length-scales are seen not to change for the majority of the recorded timescales (until $t^{+0} \approx 531.97$), after which a drastic reduction of the streamwise length-scales of UMZ 1 is seen. As the flow settles, it is noticed that the final average steady-state length-scales of UMZ 1 settle at $z/D \approx 3.5$, indicating that they may require extended timescales to fully recover to their initial steady length-scales, $z/D \approx 3.3$. This result shows agreement with the findings by Guerrero *et al.*,[11] He and Seddighi,[7] and He and Seddighi,[8] where they showed that the core region of the flow requires extended timescales to recover due to the newly generated turbulence from the wall continuing to be convected toward the core for extended timescales during the core-relaxation stage.

Upon investigating the length-scale distributions of the second fastest UMZs (UMZ 2), the third fastest UMZs (UMZ 3), the fourth fastest UMZs (UMZ 4), the fifth fastest UMZs (UMZ 5), and the sixth fastest UMZs (UMZ 6), similar trends to UMZ 1 were seen. Specifically, each spatially coherent UMZ exhibited patterns of elongation and relaxation. However, there were differences in the overall spatial extent to which each zone elongated and relaxed, and the unsteady flow stages during which elongation was particularly prominent. Figure 11 provides a comparison of the average length-scales of spatially coherent UMZs with respect to the pipe diameter (D) and viscous units (at the final steady friction Reynolds number of $Re_\tau = 670$), seen toward the beginning of each unsteady flow stage.

Based on the initial steady flow length-scale distributions of each zone (UMZ 1–6) from Fig. 11, results further confirm that spatially coherent UMZs at the pipe center are the longest out of all spatially coherent UMZs (on average, extending up to $z/D \approx 3.2$) prior to the rapid ramp-up acceleration. In contrast, in the steady flow, the spatial extent of spatially coherent UMZs drops as one gets closer to the wall, with UMZ 6 having the shortest spatial extent out of all spatially coherent UMZs (on average extending up to $z/D \approx 1.8$).

As the flow is ramped up, it is evident from the length-scale results that different spatially coherent UMZs react differently to the flow excursion. Compared to slower, near-wall coherent flow structures (UMZ 4–6), faster coherent flow structures located near the core of the pipe elongate more (UMZ 1–3). In contrast, slow coherent flow structures do not elongate as much, unlike faster coherent flow structures. This result is in agreement with findings of earlier investigations by He and Seddighi,[7] He and Seddighi,[8] Mathur *et al.*,[10] and Guerrero *et al.*[11]

Additionally, there were indications of earlier timescales of relaxation to length scales prior to the flow ramp-up of slow spatially coherent UMZs located near the wall, compared to faster spatially coherent UMZs located far from the wall. Apart from the different rates of elongation and relaxation of the spatially coherent UMZs seen, the results indicate that all spatially coherent UMZs show an elongation up to the late pre-transition stage and relax toward the end of the core-relaxation stage. UMZ 1 and UMZ 2 showed delayed signs of recovery, with them remaining elongated until later stages of the core-relaxation stage. UMZ 3–6 show early signs of recovery, starting to recover during the transition stage and almost fully recovering toward the end of the recorded timescales of the core-relaxation stage. Apart from that, based on the low-speed near wall streak visualizations at $y^{+0} \approx 7$ by Guerrero *et al.*,[11] they could see that the streaks remain unchanged during the inertial stage. An elongation of near-wall streaks and quasi-streamwise vortices is seen during the pre-transition stage, and this elongation is an attempt to preserve the angular momentum as the streamwise Reynolds shear stresses increase near the wall. Furthermore, they showed that these streaks break down and merge during the transition stage, causing the streaks to shorten. With the propagation of turbulence enhancing the turbulence levels toward the end of the core-relaxation stage, the streaks eventually recover toward the end.

IV. CONCLUSION

The structural organization of turbulent pipe flow into spatially coherent and incoherent uniform momentum zones in a rapidly accelerating flow scenario was analyzed using high-fidelity direct numerical simulation (DNS) datasets. Since all detected instantaneous UMZs consist of spatially coherent and incoherent UMZs, a methodology based on the zone modal velocities (u_m) of instantaneous UMZs similar to Laskari *et al.*[3] was utilized in isolating spatially coherent UMZs from all instantaneous UMZs detected. It was shown that the average number of instantaneous UMZs N_{UMZ} decreases as the flow rapidly accelerates up to the pre-transition stage. During the transition stage, it is seen that the average number of instantaneous zones N_{UMZ}

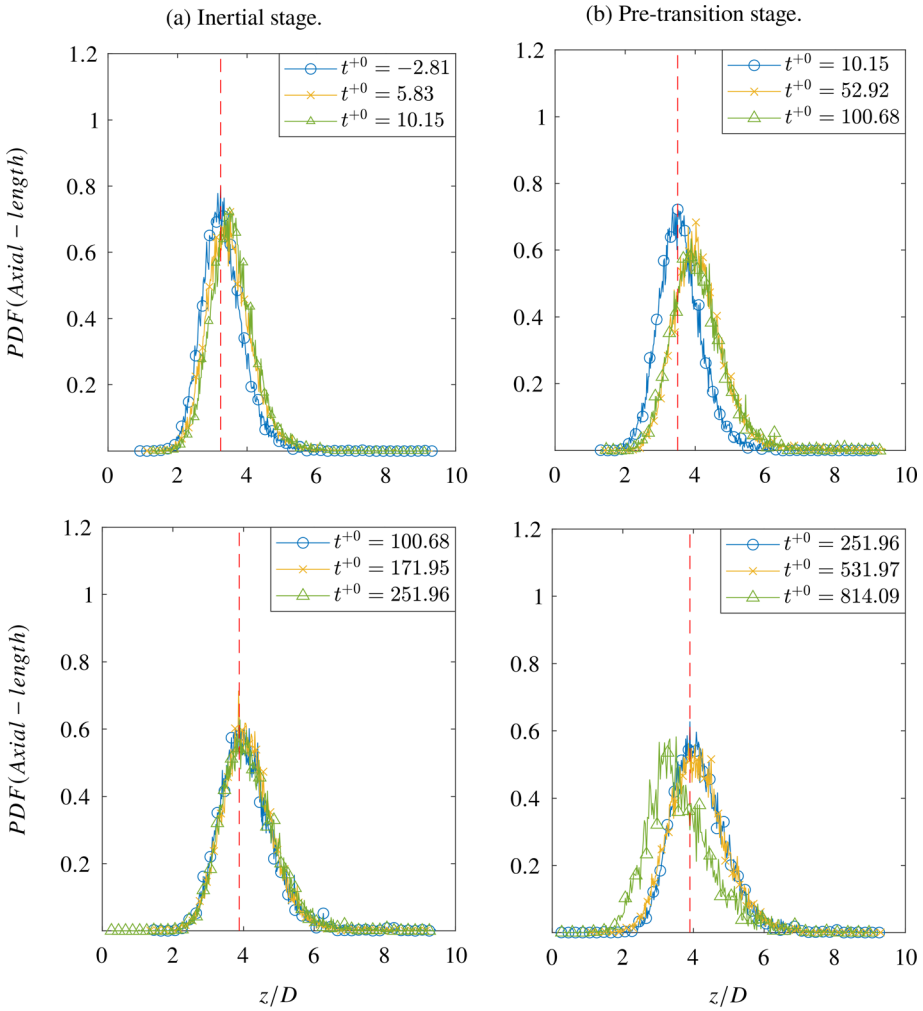

FIG. 10. PDF of zone 1 length-scales detected during the (a) inertial, (b) pre-transition, (c) transition, and (d) core-relaxation stages of the transient turbulent flow. The red dashed line (— - —) indicates the average length-scale value at the beginning of each unsteady flow stage.

increases, and toward the end of the core-relaxation stage, the average number of instantaneous zones N_{UMZ} recovers to similar levels as seen in their initial steady state. Unlike the average number of instantaneous zones N_{UMZ}, the average number of spatially coherent zones $N_{\widetilde{UMZ}}$ remained relatively unchanged during the inertial stage. During the pre-transition stage, more spatially coherent UMZs are seen, and as the flow recovers during the transition and the core-relaxation stage, the average number of spatially coherent zones $N_{\widetilde{UMZ}}$ drop and recover, similar to their initial steady flow statistics.

Upon investigating how the total number of zones identified for both spatially coherent and incoherent UMZs vary as the flow progresses through its unsteady stages, it was found that a drop in the number of zones for both spatially coherent and incoherent UMZs occur until the end of the pre-transition stage. The changes of distributions of the number of instantaneous and spatially coherent UMZs are argued to be a direct consequence of annihilation of near-wall flow structures as the flow relaminarizes during the pre-transition stage, and the formation of new complex flow patterns during the transition stage.[7,8,11] This result further indicates that there is indeed an underlying mechanism that causes merging or annihilation of zones as the flow accelerates, which influences both spatially coherent and incoherent UMZs that deserve to be explored in depth in a future study. The current authors speculate that this underlying mechanism could share similarities with the flow structural mechanisms explained by the hairpin-packet model,[1,34] as the boundaries of UMZs are of intense regions of vortical activity.[22]

When investigating the unsteady flow response of spatially coherent UMZs in terms of individual streamwise length-scales, quantitative evidence of different individual UMZs responding differently to the flow excursion was collected. It has been found that faster and closer to the pipe core, UMZs elongate the most. However, they require longer timescales to recover. Closer to the pipe wall, slower UMZs were found to be less elongated. However, they exhibit earlier signs of recovery, indicating that near-wall spatially coherent flow structures are the first to recover as the flow begins to settle, compared to near-core spatially coherent flow structures in pipes. The elongation of spatially coherent

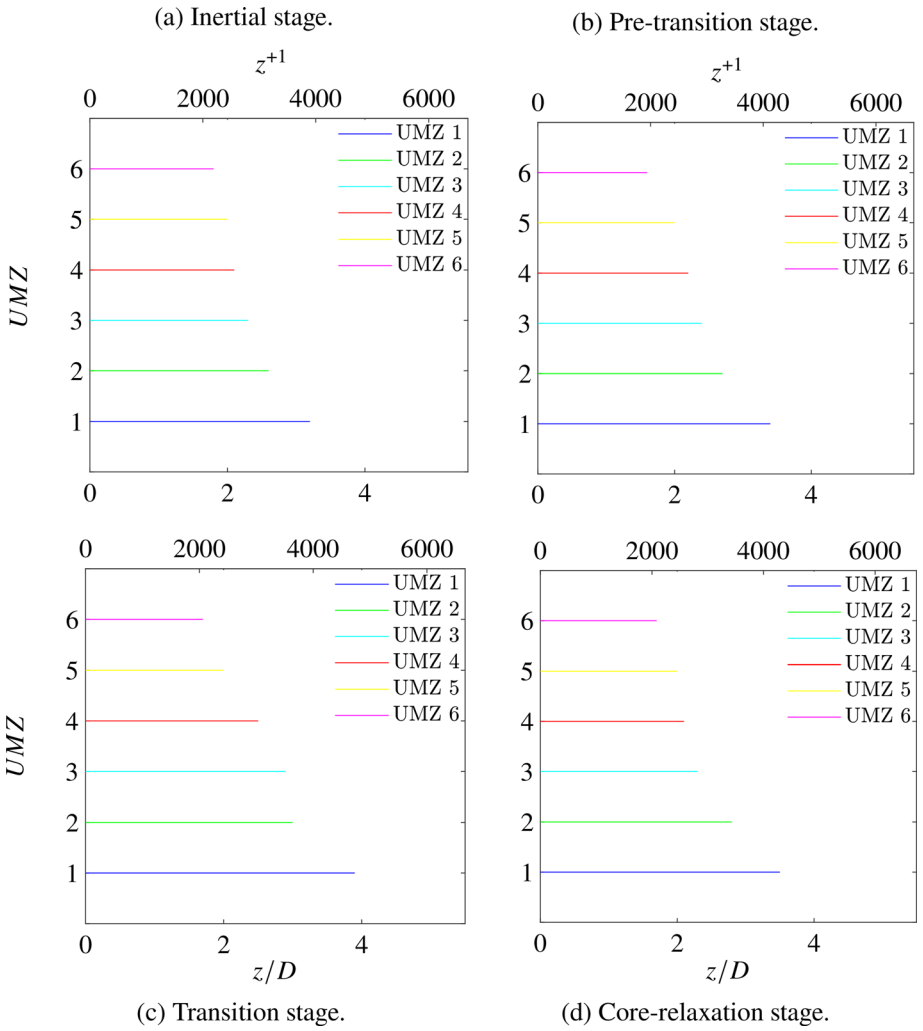

FIG. 11. A comparison between the average length-scales of spatially coherent UMZs during the (a) inertial, (b) pre-transition, (c) transition, and (d) core-relaxation stages of the transient turbulent flow. The length-scales are plotted with respect to pipe diameter (D) and in viscous units with respect to the final steady friction Reynolds number at $Re_\tau = 670$. Each colored line indicates the average length-scale value at the beginning of each unsteady flow stage.

UMZs seen predominately during the transition stage and the relaxation seen toward the core-relaxation stage of the flow are argued to be attempts by the flow structures to conserve momentum, while the asymmetry of the elongation and relaxation patterns are argued to be linked to the delay in turbulence propagation from the wall toward the core, as seen by Guerrero *et al.*,[11] in accelerating turbulent pipe flows.

ACKNOWLEDGMENTS

The authors are grateful for the transient turbulent pipe-flow datasets provided by Dr. Byron Guerrero and the HPC services at the University of Adelaide. The authors acknowledge the financial support from the Australian Research Council (ARC).

AUTHOR DECLARATIONS

Conflict of Interest

The authors have no conflicts to disclose.

Author Contributions

Isuru Gunaratne: Conceptualization (equal); Formal analysis (equal); Investigation (equal); Methodology (equal); Validation (equal); Visualization (equal); Writing – original draft (lead). **Byron Guerrero:** Conceptualization (equal); Data curation (equal); Investigation (equal); Methodology (equal); Project administration (equal); Supervision (equal); Validation (equal); Writing – review & editing (supporting). **Martin Lambert:** Conceptualization (equal); Funding acquisition (equal); Investigation (equal); Project administration (equal); Resources (equal); Supervision (equal); Writing – review & editing (supporting). **Rey Chin:** Conceptualization (equal); Formal analysis (equal); Funding acquisition (equal); Methodology (equal); Project administration (equal); Resources (equal); Supervision (equal); Writing – review & editing (supporting).

DATA AVAILABILITY

The data that support the findings of this study are available from the corresponding author upon reasonable request.

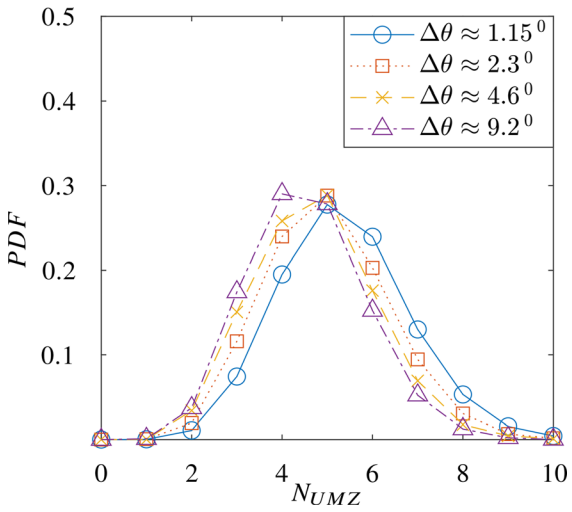

FIG. 12. Sensitivity of the volumetric wedge angle $\Delta\theta$ to the probability density function of the number of instantaneous UMZs N_{UMZ} detected at $t^{+0} = -2.8138$ (negative sign for initial steady state).

APPENDIX: SENSITIVITY ANALYSIS OF VOLUMETRIC WEDGE DIMENSIONS

When identifying UMZs based on the PDF approach, the extents of the three-dimensional flow windows considered to construct the PDFs of the streamwise velocity play a major role in the overall number of instantaneous UMZs detected, as larger flow windows become, local PDF peaks may not be identified distinctly.[2]

For the current work, a streamwise window size of $0.5R$ was selected, similar to the integration window size from Laskari *et al.*[3] and a sensitivity test was conducted to determine the maximum azimuthal extent $\Delta\theta$ of each volumetric flow wedge, while the peak of the PDF of N_{UMZ} is preserved at 5 prior to the flow acceleration, matching the distribution peak by Chen *et al.*,[2] (peak at 5), due to comparable initial steady state friction Reynolds numbers at $Re_\tau = 500$. Figure 12 demonstrates the results from the sensitivity test conducted, and as it is evident, the maximum azimuthal extent to which the peak of the PDF of N_{UMZ} is preserved at 5 was found to be at $\Delta\theta \approx 4.6^\circ$.

REFERENCES

[1]R. J. Adrian, C. D. Meinhart, and C. D. Tomkins, "Vortex organization in the outer region of the turbulent boundary layer," J. Fluid Mech. **422**, 1–54 (2000).
[2]X. Chen, Y. M. Chung, and M. Wan, "Uniform-momentum zones in a turbulent pipe flow," J. Fluid Mech. **884**, A25 (2020).
[3]A. Laskari, R. de Kat, R. J. Hearst, and B. Ganapathisubramani, "Time evolution of uniform momentum zones in a turbulent boundary layer," J. Fluid Mech. **842**, 554–590 (2018).
[4]T. Maruyama, T. Kuribayashi, and T. Mizushina, "The structure of the turbulence in transient pipe flows," J. Chem. Eng. Jpn. **9**, 431–439 (1976).
[5]D. Greenblatt and E. A. Moss, "Rapid temporal acceleration of a turbulent pipe flow," J. Fluid Mech. **514**, 65–75 (2004).
[6]S. He, C. Ariyaratne, and A. E. Vardy, "Wall shear stress in accelerating turbulent pipe flow," J. Fluid Mech. **685**, 440–460 (2011).
[7]S. He and M. Seddighi, "Turbulence in transient channel flow," J. Fluid Mech. **715**, 60–102 (2013).
[8]S. He and M. Seddighi, "Transition of transient channel flow after a change in Reynolds number," J. Fluid Mech. **764**, 395–427 (2015).
[9]A. Mathur, "Study of accelerating and decelerating turbulent flows in a channel," Ph.D. thesis (The University of Sheffield, 2016).
[10]A. Mathur, S. Gorji, S. He, M. Seddighi, A. E. Vardy, T. O'Donoghue, and D. Pokrajac, "Temporal acceleration of a turbulent channel flow," J. Fluid Mech. **835**, 471–490 (2018).
[11]B. Guerrero, M. F. Lambert, and R. C. Chin, "Transient dynamics of accelerating turbulent pipe flow," J. Fluid Mech. **917**, A43 (2021).
[12]B. Guerrero, M. F. Lambert, and R. C. Chin, "Extension of the 1D unsteady friction model for rapidly accelerating and decelerating turbulent pipe flows," J. Hydraul. Eng. **148**, 04022014 (2022).
[13]B. Guerrero, M. F. Lambert, and R. C. Chin, "Transient behaviour of decelerating turbulent pipe flows," J. Fluid Mech. **962**, A44 (2023).
[14]T. Theodorsen, "Mechanisms of turbulence," in Proceedings of the 2nd Midwestern Conference on Fluid Mechanics, 1952.
[15]S. J. Kline, W. C. Reynolds, F. A. Schraub, and P. W. Runstadler, "The structure of turbulent boundary layers," J. Fluid Mech. **30**, 741–773 (1967).
[16]M. R. Head and P. Bandyopadhyay, "New aspects of turbulent boundary-layer structure," J. Fluid Mech. **107**, 297–338 (1981).
[17]G. L. Brown and A. S. W. Thomas, "Large structure in a turbulent boundary layer," Phys. Fluids **20**, S243–S252 (1977).
[18]K. T. Christensen and R. J. Adrian, "Statistical evidence of hairpin vortex packets in wall turbulence," J. Fluid Mech. **431**, 433–443 (2001).
[19]B. Ganapathisubramani, E. K. Longmire, and I. Marusic, "Characteristics of vortex packets in turbulent boundary layers," J. Fluid Mech. **478**, 35–46 (2003).
[20]R. J. Adrian, "Hairpin vortex organization in wall turbulence," Phys. Fluids **19**, 041301 (2007).
[21]K. C. Kim and R. J. Adrian, "Very large-scale motion in the outer layer," Phys. Fluids **11**, 417–422 (1999).
[22]D. Meinhart and R. J. Adrian, "On the existence of uniform momentum zones in a turbulent boundary layer," Phys. Fluids **7**, 694–696 (1995).
[23]X. Chen, Y. M. Chung, and M. Wan, "The uniform-momentum zones and internal shear layers in turbulent pipe flows at Reynolds numbers up to $Re_\tau = 1000$," Int. J. Heat Fluid Flow **90**, 108817 (2021).
[24]M. Gul, G. E. Elsinga, and J. Westerweel, "Internal shear layers and edges of uniform momentum zones in a turbulent pipe flow," J. Fluid Mech. **901**, A10 (2020).
[25]K. Horiuti and Y. Takagi, "Identification method for vortex sheet structures in turbulent flows," Phys. Fluids **17**, 121703 (2005).
[26]D. Fan, J. Xu, M. X. Yao, and J. P. Hickey, "On the detection of internal interfacial layers in turbulent flows," J. Fluid Mech. **872**, 198–217 (2019).
[27]Y. S. Kwon, J. Philip, C. M. De Silva, N. Hutchins, and J. P. Monty, "The quiescent core of turbulent channel flow," J. Fluid Mech. **751**, 228–254 (2014).
[28]C. M. De Silva, N. Hutchins, and I. Marusic, "Uniform momentum zones in turbulent boundary layers," J. Fluid Mech. **786**, 309–331 (2016).
[29]P. Fischer, G. Kruse, and F. Loth, "Spectral element methods for transitional flows in complex geometries," J. Sci. Comput. **17**, 81–98 (2002).
[30]B. Guerrero, M. F. Lambert, and R. C. Chin, "Extreme wall shear stress events in turbulent pipe flows: Spatial characteristics of coherent motions," J. Fluid Mech. **904**, A18 (2020).
[31]S. He and J. D. Jackson, "A study of turbulence under conditions of transient flow in a pipe," J. Fluid Mech. **408**, 1–38 (2000).
[32]C. Chin, A. S. H. Ooi, I. Marusic, and H. M. Blackburn, "The influence of pipe length on turbulence statistics computed from direct numerical simulation data," Phys. Fluids **22**, 115107 (2010).
[33]R. Narasimha and K. R. Sreenivasan, "Relaminarization in highly accelerated turbulent boundary layers," J. Fluid Mech. **61**, 417–447 (1973).
[34]J. Zhou, R. J. Adrian, S. Balachandar, and T. M. Kendall, "Mechanisms for generating coherent packets of hairpin vortices in channel flow," J. Fluid Mech. **387**, 353–396 (1999).